Applied Physics Reviews

Two-dimensional flexible thermoelectric devices: Using modeling to deliver optimal capability

Cite as: Appl. Phys. Rev. **8**, 041404 (2021); https://doi.org/10.1063/5.0067930
Submitted: 20 August 2021 • Accepted: 23 September 2021 • Published Online: 15 October 2021

Shengduo Xu, Min Hong, Meng Li, et al.

Applied Physics Reviews ARTICLE scitation.org/journal/are

Two-dimensional flexible thermoelectric devices: Using modeling to deliver optimal capability

Cite as: Appl. Phys. Rev. **8**, 041404 (2021); doi: 10.1063/5.0067930
Submitted: 20 August 2021 · Accepted: 23 September 2021 ·
Published Online: 15 October 2021

Shengduo Xu,[1] Min Hong,[2] Meng Li,[1] Qiang Sun,[3] Yu Yin,[1] Weidi Liu,[2] Xiaolei Shi,[2] Matthew Dargusch,[1] Jin Zou,[1,3,a)] and Zhi-Gang Chen[1,2,a)]

AFFILIATIONS

[1]Materials Engineering, University of Queensland, Brisbane, Queensland 4072, Australia
[2]Centre for Future Materials, University of Southern Queensland, Springfield Central, Queensland 4300, Australia
[3]Centre for Microscopy and Microanalysis, University of Queensland, Brisbane, Queensland 4072, Australia

[a)]Authors to whom correspondence should be addressed: j.zou@uq.edu.au and zhigang.chen@usq.edu.au

ABSTRACT

Two-dimensional flexible thermoelectric devices (2D FTEDs) are a promising candidate for powering wearable electronics by harvesting low-grade energy from human body and other ubiquitous energy sources. However, immature device designs in the parametric geometries of FTEDs cannot provide an optimized output power density because of either insufficient temperature difference or unnecessarily large internal resistance. Here, we theoretically design optimal parametric geometries of 2D FTEDs by systematically considering applied temperature difference, temperature-dependent thermoelectric properties of materials, leg thickness, and thermodynamic conditions. The obtained analytical solution determines the optimal leg length for 2D FTEDs when these parameters are given and, therefore, minimizes the internal device resistance and simultaneously maintains the high temperature difference across the TE legs to maximize the device output power density. According to this design, we use flexible Ag_2Se films as thermoelectric legs to assemble a 2D FTED, which displays a maximum power output of 11.2 mW and a normalized output power density of 1.43 μW cm^{-2} K^{-1} at a temperature difference of 150 K, outnumbering other 2D FTEDs by threefolds. Our 2D FTED can power up four light-emitting diodes, which shows great potential for harvesting electricity from low-grade heat. The exotic and reliable device design concept of 2D FTEDs reported here can be extended to other thermoelectric systems to boost the practical applications of FTEDs.

INTRODUCTION

Advances in self-powered electronic technologies are providing new opportunities in a range of applications, including healthcare,[1] human–machine interaction,[2] linking devices, and Internet of Things (IoT).[3] Ubiquitous energy sources, such as solar energy,[4] mechanical energy,[5] chemical energy,[5] thermal energy, or even the human body,[6] can be converted into electricity to self-power up the electronic devices. Different energy harvesting devices, such as solar cells,[7,8] piezoelectric devices,[9] and thermoelectric devices (TEDs),[10–12] have been designed to form integrated and self-powered systems. Particularly, TEDs, featured with silence and no moving parts, are favorable in harvesting electricity from low-grade heat.

Two-dimensional (2D) flexible TEDs (FTEDs), usually consisting of 2D FTE films, are now attract significant attention.[13] 2D FTEDs can be used in various curved surfaces and show negligible demands for working space. Unlike the traditional bulk TEDs that require either long TE legs or an extra cooling system to achieve a large temperature difference (ΔT), 2D FTEDs sustain large ΔT in short legs without extra cooling systems because of their relatively large specific surface areas,[14] which promotes the miniaturization of the power generators. With regard to material availability, the 2D FTE films can be fabricated using various organic and inorganic TE materials with promising thermoelectric performance, which is evaluated by the dimensionless figure-of-merit (ZT): $ZT = S^2\sigma T/\kappa$, where σ is the electrical conductivity, S is the Seebeck coefficient, κ is the thermal conductivity (including electron κ_e and lattice κ_l components), T is the absolute temperature, and $S^2\sigma$ is the power factor.[15,16] Typical organic TE materials are conducting polymers with relatively high thermoelectric performance.[17–21] For example, poly(3,4-ethylenedioxythiophene) (PEDOT) family shows a high ZT of 0.42,[22] and polyaniline (PANI) family presents an ultra-high $S^2\sigma$ of 1825 μW m^{-1} K^{-2}.[19] Another newly reported self-healable ionic copolymer film even shows a tremendous ZT of 1.04 with ultra-high S in a suitable humidity.[23] Apart from the conducting polymers, some inorganic–organic hybrid materials also present both excellent TE performance and good flexibility as these hybrid materials combine the merits of both the inorganic fillers and the polymer matrices.[24–26] Moreover, inorganic semiconductors can also steadily exist in the form of flexible 2D films.[27,28] Recently, flexible Ag_2Se 2D films were reported to secure an ultra-high $S^2\sigma$ of 2231.5 μW m^{-1} K^{-2} and have been proved to be applicable in the 2D FTEDs.[27,28] Despite these inspiring advances in TE materials, their engineering applications have been left far behind due to the low device performance. The highest normalized output power density (p_m, i.e., the amount of output power per area per Kelvin) of 2D FTEDs achieved so far is only 0.01 μW cm^{-2} K^{-1} (calculated using working surface areas instead of cross-sectional areas),[29] which is far too small to power up milliwatt electronics. The main reason is the immature device design, which generally ignores the geometry optimization for maximizing p_m of 2D FTEDs.

In this study, aiming to minimize the internal resistance (R_{in}) and simultaneously maintain the high ΔT, we develop a device design model to optimize the geometry of 2D FTEDs so as to maximize p_m. Based on our theoretical calculations by systematically considering four key factors, namely, the temperature difference, the TE properties, leg dimensions, and thermodynamic conditions of devices, we determine the transition length (Δx) of the applied temperature difference in the thermoelectric leg. Δx can be the optimal length of the TE leg to minimize the R_{in} of corresponding 2D FTEDs. Guided by this innovative device design, 2D FTEDs are experimentally assembled by using flexible Ag_2Se films with a stable average power factor ($\overline{PF}$) of ~1350 μW m^{-1} K^{-2} between 300 and 450 K. The as-developed 2D FTED can generate an output power of 11.2 mW and a p_m of 1.43 μW cm^{-2} K^{-1} at a ΔT of 150 K, which can provide power suitable for milliwatt electronics, such as light-emitting diodes (LEDs).

RESULTS AND DISCUSSION

Assembly procedure for 2D FTEDs

Geometry optimization of the TE leg is critical in the design and fabrication of 2D FTEDs, since an optimal leg length enables the TE

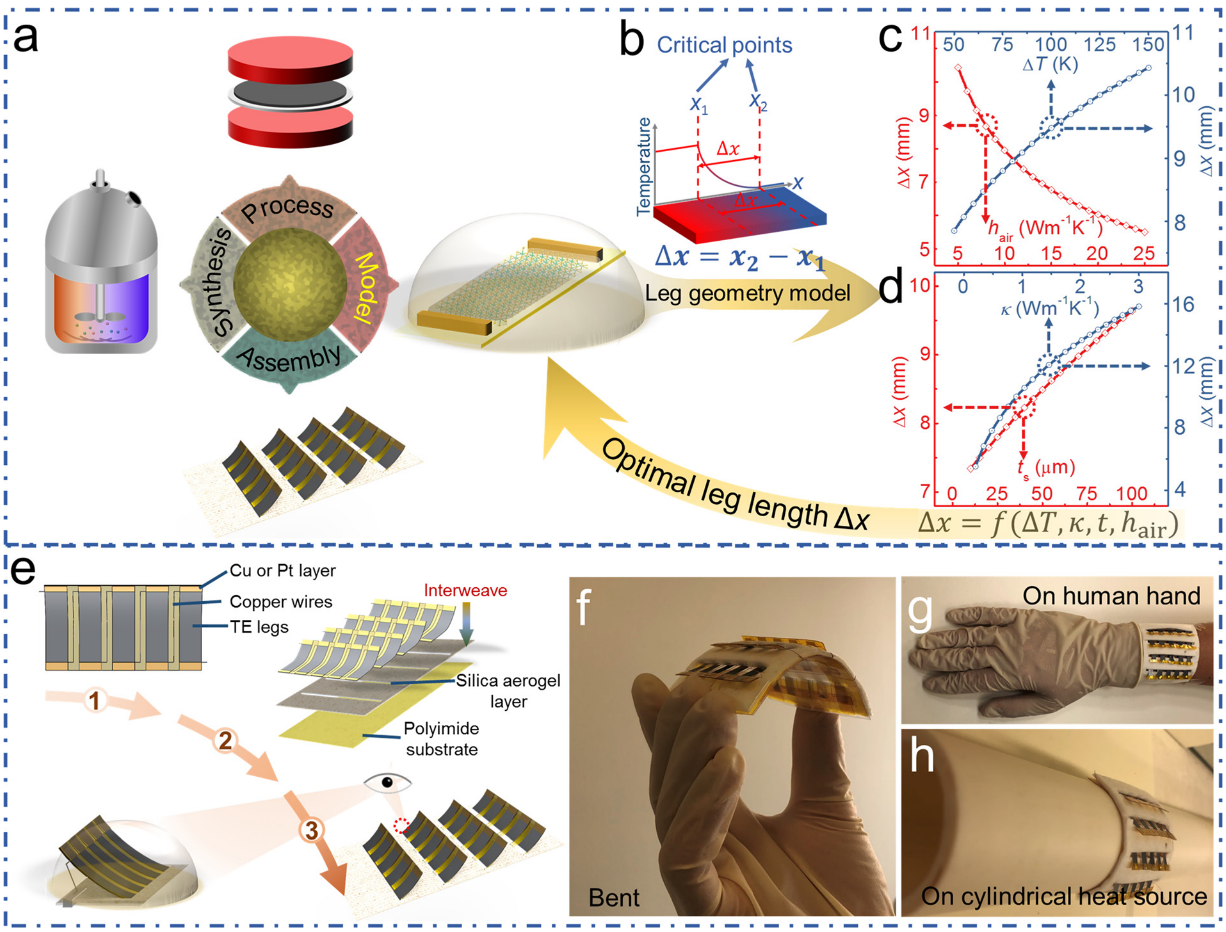

FIG. 1. (a) Routine of fabricating a 2D FTED. Ag_2Se nanowires were synthesized using the solution method, followed by a hot sintering process to fabricate Ag_2Se films. The as-fabricated films will be further used in the assembly of 2D FTEDs; (b) schematic diagram of temperature distribution on a TE leg. The temperature gradient at the critical points x_1 and x_2 is set to be 1 K m^{-1}, suggesting temperature is stable at the critical points. The optimal leg length Δx is defined as the distance between x_1 and x_2; (c) and (d) Δx as a function of h_{air}, ΔT, t_s, and κ; and (e) diagram of the assembly of a 2D FTED. To form the unit, thermoelectric legs were connected by copper wires in series, and contact resistance was reduced by the addition of evaporated Cu or Pt layers between the copper wire and the thermoelectric leg. To obtain a large output power, five of these units were interweaved through an aerogel layer made of silica and were secured using adhesive polyimide substrate; (f), (g), and (h) digital photographs of 2D FTEDs.

leg to provide utmost p_m by securing sufficient ΔT and the smallest R_{in}. Figure 1(a) illustrates the procedure adopted in the fabrication of a 2D FTED, which involves material synthesis, thin-film processing, geometry optimization, and device assembly. The details of the first two steps can be found in the supplementary material. At the third stage, a leg geometry model is applied to determine the optimal Δx by systematically considering the impacts of ΔT, κ, t_s (TE material thickness), and h_{air} (natural convection coefficient), based on our developed equations in (S1). Figure 1(b) schematically displays the temperature distribution in a TE leg. Qualitatively, the temperature change completes within the temperature transition area from critical points x_1 to x_2, and the length between x_1 and x_2 is defined as Δx.[14] Then, to ensure a low R_{in} of 2D FTEDs, the optimal length of the TE leg should equal Δx. Figures 1(c) and 1(d) show the evolution of Δx with ΔT, κ, t_s, and h_{air}. Δx is positively correlated with ΔT, κ, and t_s because smoothened temperature distribution curves (shown in Fig. S1) correspond to larger ΔT, κ, and t_s. On the other hand, increasing h_{air} narrows the temperature transition area (shown in Fig. S1), leading to a smaller Δx, since strong heat convection accelerates the temperature transition. These simulation results determine Δx for a TE leg made of a certain material (κ and t_s) under working conditions (ΔT and h_{air}). Figure 1(e) shows the assembly procedure of a 2D FTED. The as-designed TE legs were connected by copper wires in series to form a unit. To reduce the contact resistance between the copper wire and the TE legs, two Cu or Pt layers were evaporated on the top and bottom sides of each leg, respectively. Five units interweave through a layer of silica aerogel to maintain ΔT. In addition, another adhesive polyimide substrate was further attached to the bottom surface of the 2D FTEDs to fasten the TE legs. Notably, every two units were connected in series to ensure sufficient output voltage. Figures 1(f)–1(h) show the photographs of the as-fabricated 2D FTEDs. The excellent flexibility enables 2D FTEDs to be adapted on curved surfaces such as the human hand or other cylindrical heat sources.

Leg geometry model for 2D FTEDs

Based on the determined Δx, we calculated p_m upon an external loading equivalent to the internal resistance of the 2D FTED as $p_m = \frac{\overline{PF}\, t_s \Delta T}{4\Delta x^2}$. Here, $\overline{PF}$ is the average power factor and can be expressed as $\overline{PF} = \frac{\left(\int_{T_1}^{T_h} S(T)dT/\Delta T\right)^2}{\int_0^{\Delta x} \sigma(x)^{-1} dx/\Delta x}$. The energy efficiency η is the ratio of output power to the sum of output power and heat flux that is transferred from the heat source to the device. Notably, we also considered the heat loss caused by convection and radiation, which are usually ignored in a few previous reports.[30,31] η can be expressed as $\eta = \frac{P}{P+Q} = \frac{p_m \Delta T \Delta x}{p_m \Delta T \Delta x + t\kappa T'(x)|_{x=x_1}}$, where P and Q represent the output power of the 2D FTEDs and the heat flux transferring from the heat source to the device and $T'(x)|_{x=x_1^+}$ represents the temperature gradient at the right side of the critical point x_1. All the detailed calculations are included in the supplementary material.

Notably, Δx, p_m, and η produced by the proposed model vary from different TE materials. We selected flexible Ag_2Se films as our leg

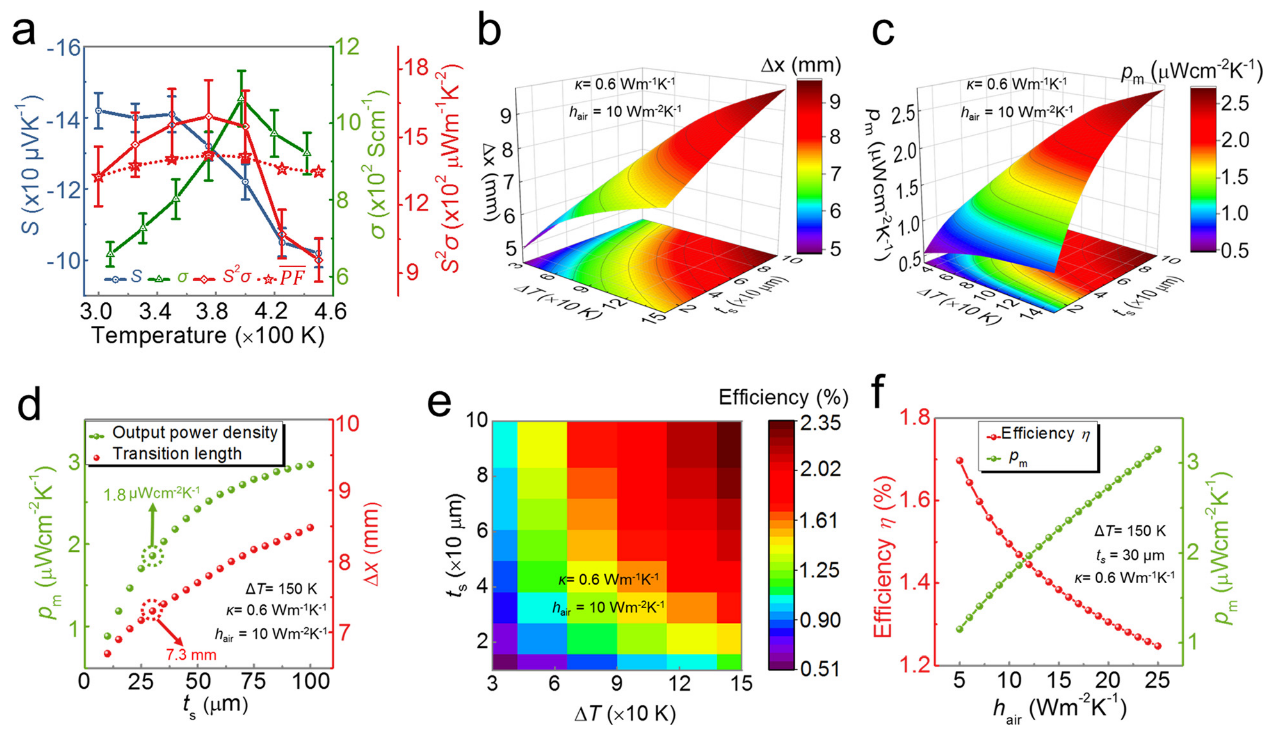

FIG. 2. (a) TE properties of as-prepared Ag_2Se film. The red dotted line stands for the average power factor $\overline{PF}$; the color-maps of Δx (b) and p_m (c) as functions of ΔT and t_s; (d) p_m and Δx as functions of t_s when ΔT, κ, and h_{air} equal, respectively, 150 K, 0.6 W m^{-1} K^{-1}, and 10 W m^{-2} K^{-1}; (e) the color-map of η as functions of ΔT and t_s; and (f) p_m and η as functions of h_{air} when ΔT, κ, and t_s equal, respectively, 150 K, 0.6 W m^{-1} K^{-1}, and 30 μm.

materials to understand the design of devices. The procedure for the preparation of Ag_2Se films is available in the supplementary material, and their typical TE properties can be seen in Fig. 2(a). As can be seen, σ (green curve) increases with increasing temperature before 400 K and then decreases afterward. Unlike σ, S (blue curve) monotonically decreases from 300 to 450 K. As a result, the $S^2\sigma$ (red curve) shows a bump-like tendency with increasing temperature and reaches the peak value of 1578 μW m^{-1} K^{-2} at 400 K. The calculated $\overline{PF}$ (red dotted curve) fluctuates at around 1350 μW m^{-1} K^{-2} with various T_h. The in-plane κ of the Ag_2Se film is reported to be 0.6 W m^{-1} K^{-1}.[27] Moreover, h_{air} is set as 10 W m^{-2} K^{-1}, corresponding to a typical working environment of the 2D FTED.[32] As a result, Figs. 2(b) and 2(c) show the color-maps of Δx and p_m as functions of t_s and ΔT, respectively. Both Δx and p_m increase with larger t_s, indicating that a thicker Ag_2Se layer yields better output performance. Notably, the t_s of the as-prepared Ag_2Se layer is measured to be 30 μm on the cross-sectional SEM image shown in Fig. S2. Thus, our Δx and p_m are determined to be 7.3 mm and 1.8 μW cm^{-2} K^{-1}, respectively, as can be seen in Fig. 2(d). Figure 2(e) shows the color-map of η as functions of ΔT and t_s in the 2D FTED. η of the Ag_2Se-based 2D FTED is predicted to be about 1.7% under a ΔT of 150 K. Increasing t_s of the Ag_2Se layer to 100 μm can further improve η to 2.35%. Interestingly, p_m and η are reversely dependent on h_{air}, as shown in Fig. 2(f). The 2D FTED shows an increasing p_m with larger h_{air}, derived from the decreased Δx due to the strong heat convection, whereas η decreases with h_{air} since more energy can be wasted by contact with the air.

Device performance of 2D FTED

Our calculation results suggest an optimal Δx of 7.3 mm for the as-prepared Ag_2Se films under a ΔT of 150 K. To verify this prediction, an experiment was carried out, and the results are shown in Fig. 3(a), which presents the thermal infrared image of an Ag_2Se film heated up to 180 °C. The enlarged image indicates that the temperature decreases from 180 °C rapidly to room temperature, spanning a length of ~7.5 mm, and this matches well with our predicted Δx of 7.3 mm. This infrared image proves the validity of our model. Therefore, the sintered Ag_2Se films were tailored accordingly into rectangular pieces whose length and width are 7.5 and 5 mm, respectively. Based on these pieces, we assembled a 2D FTED using 142 TE legs in total connecting in series with a total area of 52 cm^{-2}. The measured R_{in} in our 2D FTED is as low as 120.8 Ω. Such a 2D FTED can power up four LEDs

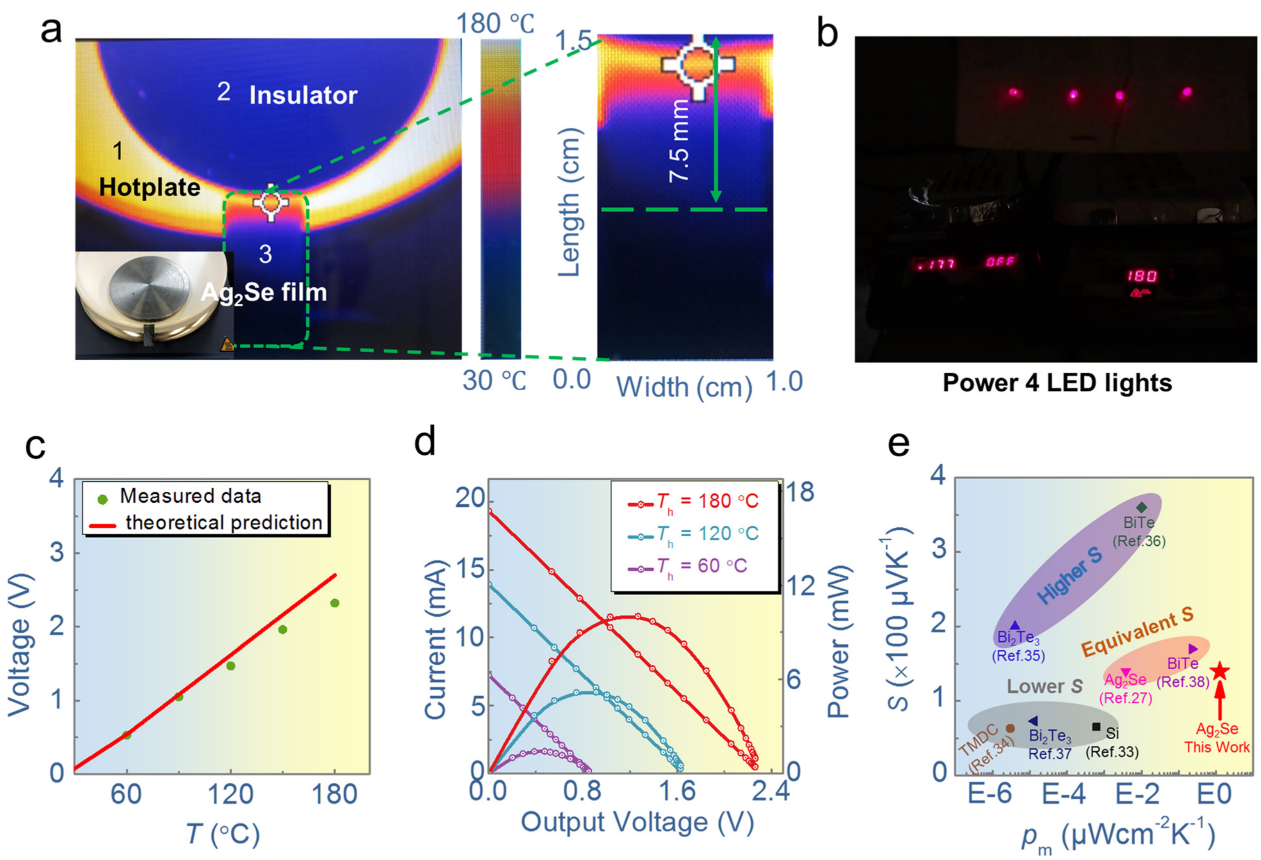

FIG. 3. (a) The thermal infrared image of a Ag_2Se film heated at 180 °C. The inset is the corresponding digital image, where the white surface is the surface of hot plate, the black film is the Ag_2Se film suppressed by a layer of silica aerogel layer and heavy stainless steel; (b) four LED lights were powered when the two dimensional (2D) flexible thermoelectric device (FTED) was heated at 180 °C; (c) the theoretical and measured output voltage as a function of hot-end temperature; (d) the current and output power as functions of output voltage. The data were measured when temperature of the hot plate was set to be 60, 120, and 180 °C; and (e) the performance comparison between the recent state-of-the-art flexible/wearable TEGs and this work.

at the ΔT of 150 K, as indicated in Fig. 3(b). Figure 3(c) presents the open-circuit temperature-dependent voltage. The measured voltage deviates from the calculated theoretical values when the temperatures are beyond 120 °C, suggesting that the real ΔT is smaller than the applied ΔT from the heating source. This phenomenon can be attributed to the insufficient thermal insulation provided by the silica aerogel layer with a thickness of only 5 mm. To achieve better thermal insulation, a thicker substrate or a vertical alignment topology of the TE legs could be applied. As a result, a maximum output power of 11.2 mW can be generated in the 2D FTED heated at 180 °C when the loaded resistance equals the R_{in} of the 2D FTED, as shown in Fig. 3(d). Such high output power is sufficient to drive milliwatt electronics. Moreover, the linear relations between the current and the voltage indicate that Ohmic contact existed in the electrodes and TE films. Moreover, the milliwatt level power generation can also be secured by a much smaller ΔT of 30 K, suggesting the potential practical applications with small temperature drop. Figure 3(e) plots the comparison between the state-of-the-art flexible/wearable TEDs and our work.[27,33–38] S of the Ag_2Se film is not the highest one, yet the rational device design method enables our 2D FTED to produce the highest measured p_m of 1.43 μW cm^{-2} K^{-1}. Noteworthy, the measured p_m is quite close to the predicted value of 1.8 μW cm^{-2} K^{-1}, verifying the reliability of our device design.

Flexibility and stability of 2D FTED

In addition to the high p_m, mechanical robustness and thermal stability are also important to ensure the long-term steady operation of the 2D FTED. To evaluate the mechanical flexibility and thermal stability of our 2D FTEDs, we perform both bending and heating-cooling tests.[39,40] Figure 4(a) shows the resistance change of our TE leg and the output power change of the 2D FTED under various curve radius. The resistance change of the TE leg decreases from 15% to 0% when the curve radius enlarged from 6 to 15 mm. On the other hand, our 2D FTED also shows excellent operation stability, evidenced by the stable output power when being attached to cylindrical objects with a radius from 30 to 44 mm and heated at 100 °C (details of the measurement can be seen in the supplementary material). To further investigate how the TE properties evolve with increasing bending cycles, we measured the TE properties of one leg after bending under a radius of 15 mm for 1000 cycles, as shown in Fig. 4(b). Both σ and S can be maintained even after 1000 bending cycles, demonstrating the stable TE properties as well as excellent flexibility of the Ag_2Se films. We also measured σ and S of the Ag_2Se films for 20 heating and cooling cycles, and the results are plotted in Figs. 4(c) and 4(d). As can be seen, no obvious fluctuation of temperature-dependent σ and S can be observed in 20 heating and cooling cycles, which suggests that our module possesses excellent thermal stability and reversibility for long-term operation.

CONCLUSIONS

In conclusion, a new device design has been developed for 2D FTEDs to achieve milliwatt output power by considering the TE properties of the materials, leg geometry, and thermodynamic conditions. According to our design, we can predict an optimal leg length of

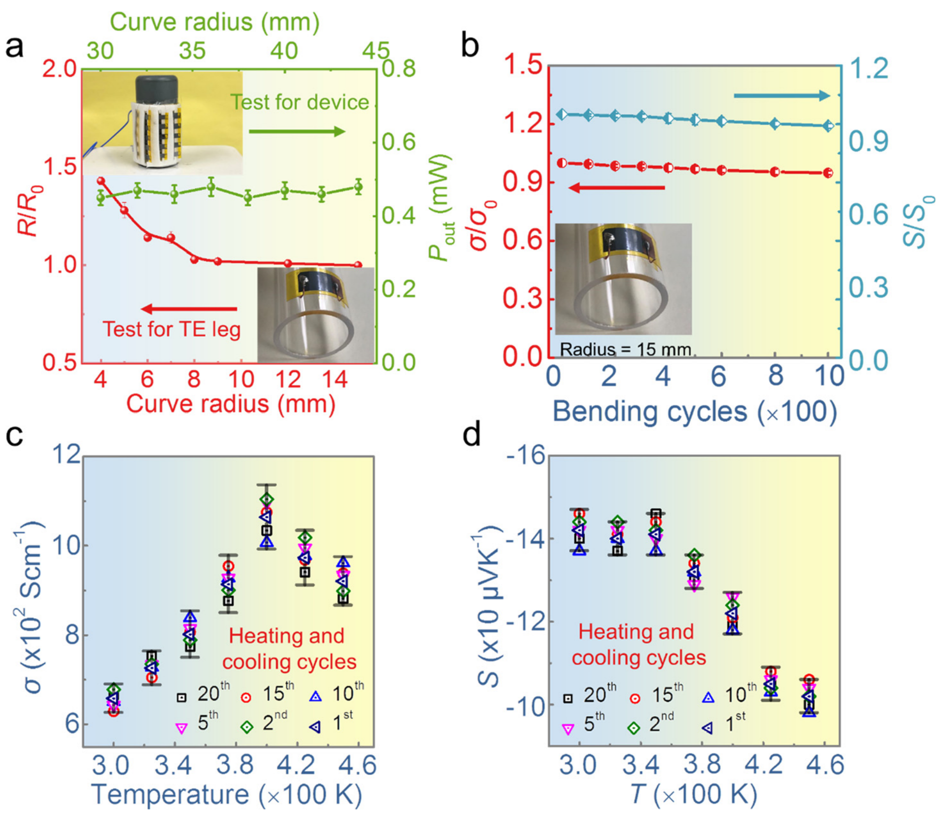

FIG. 4. (a) The resistance change of the Ag_2Se leg (red) and the output power change of the 2D FTED (green) under various curve radius. The left-top inset and right-bottom insets correspond to the images of 2D FTED and Ag_2Se film, respectively; (b) the TE properties of the TE leg after bending under a radius of 15 mm for 1000 cycles. The left-bottom inset corresponds to digital image of Ag_2Se film; the σ (c) and S (d) of the films for 20 heating and cooling cycles, respectively.

7.3 mm to achieve a high p_m of 1.8 μW cm^{-2} K^{-1} for the as-prepared Ag_2Se films with ΔT of 150 K and h_a of 10 W m^{-2} K^{-1}. Based on this model, a 2D FTED, assembled by the as-designed Ag_2Se legs, shows a high open-circuit voltage of 2.32 V at a ΔT of 150 K. As a result, the 2D FTED experimentally supplies a maximum output power of 11.2 mW, successfully powering up four LEDs. Moreover, a high p_m of 1.43 μW cm^{-2} K^{-1} can be obtained, which is much larger than that of other 2D FTEDs. This work offers a rational and reliable device design model to achieve milliwatt output power in 2D FTEDs by harvesting electricity from low-grade heat.

METHODS

Synthesis of Ag_2Se

Details of the synthesis of Ag_2Se nanowires can be seen in the supplementary material. The as-prepared Ag_2Se nanowires powder was filtered onto porous nylon membranes to fabricate Ag_2Se films using vacuum-assisted filtration equipment. Then, the Ag_2Se films were dried out in a vacuum oven at 70 °C overnight before they were hot-pressed at 200 °C under 1 MPa for 30 min.

Measurement and characterization

Both σ and S of the samples were measured using an SBA 458 (Netzsch). The Van der Pauw method in a magnetic field up to ±1.5 T was used to measure n_H and μ_H. The x-ray diffractometer of Bruker D8 Advance MKII was employed to collect the XRD patterns of the Se and Ag_2Se nanowires. JEOL 7001F was utilized to observe the morphologies of the Se, Ag_2Se nanowires, and the Ag_2Se films. Hitachi HF5000 was applied to characterize the microstructure of the Ag_2Se nanowires.

Device fabrication

The hot-pressed Ag_2Se films were cut into strips (12 × 10 mm^2) whose two ends (leaving the middle 7.3 mm-long section sheltered) were coated with a 200 nm-thick layer of copper via a mask and evaporation. After that, each strip was connected by copper wires by tin soldering. All these strips were interwoven through a layer of silica aerogel sheet connecting in series to obtain a 2D FTED. The output voltage and internal resistance of the 2D FTED were measured by a multimeter.

SUPPLEMENTARY MATERIAL

See the supplementary material for a detailed description of device modeling and experimental procedures.

ACKNOWLEDGMENTS

The authors acknowledge the financial support provided by the Australia Research Council and the USQ Strategic research fund. Shengduo Xu acknowledges the China Scholarship Council for providing the Ph.D. stipend. The Australian Microscopy and Microanalysis Research Facility is acknowledged for providing the characterization facilities.

DATA AVAILABILITY

The data that support the findings of this study are available from the corresponding authors upon reasonable request.

REFERENCES

[1]T. Ding, K. H. Chan, Y. Zhou, X. Q. Wang, Y. Cheng, T. Li, and G. W. Ho, Nat. Commun. **11**, 6006 (2020).
[2]K. Sim, Z. Rao, Z. Zou, F. Ershad, J. Lei, A. Thukral, J. Chen, Q.-A. Huang, J. Xiao, and C. Yu, Sci. Adv. **5**, eaav9653 (2019).
[3]B. Lee, H. Cho, K. T. Park, J. S. Kim, M. Park, H. Kim, Y. Hong, and S. Chung, Nat. Commun. **11**, 5948 (2020).
[4]S. Park, S. W. Heo, W. Lee, D. Inoue, Z. Jiang, K. Yu, H. Jinno, D. Hashizume, M. Sekino, T. Yokota, K. Fukuda, K. Tajima, and T. Someya, Nature **561**, 516–521 (2018).
[5]C. Xu, Y. Song, M. Han, and H. Zhang, Microsyst. Nanoeng. **7**, 25 (2021).
[6]Y. Wang, L. Yang, X. L. Shi, X. Shi, L. Chen, M. S. Dargusch, J. Zou, and Z. G. Chen, Adv. Mater. **31**, e1807916 (2019).
[7]B. J. Kim, D. H. Kim, Y.-Y. Lee, H.-W. Shin, G. S. Han, J. S. Hong, K. Mahmood, T. K. Ahn, Y.-C. Joo, K. S. Hong, N.-G. Park, S. Lee, and H. S. Jung, Energy Environ. Sci. **8**, 916–921 (2015).
[8]J. Yoon, A. J. Baca, S. I. Park, P. Elvikis, J. B. Geddes, L. Li, R. H. Kim, J. Xiao, S. Wang, T. H. Kim, M. J. Motala, B. Y. Ahn, E. B. Duoss, J. A. Lewis, R. G. Nuzzo, P. M. Ferreira, Y. Huang, A. Rockett, and J. A. Rogers, Nat. Mater. **7**, 907–915 (2008).
[9]Z. L. Wang, J. Chen, and L. Lin, Energy Environ. Sci. **8**, 2250–2282 (2015).
[10]R. Venkatasubramanian, E. Siivola, T. Colpitts, and B. O'Quinn, Nature **413**, 597–602 (2001).
[11]S. Roychowdhury, T. Ghosh, R. Arora, M. Samanta, L. Xie, N. K. Singh, A. Soni, J. He, U. V. Waghmare, and K. Biswas, Science **371**, 722–727 (2021).
[12]T. Ghosh, S. Roychowdhury, M. Dutta, and K. Biswas, ACS Energy Lett. **6**, 2825–2837 (2021).
[13]X. L. Shi, J. Zou, and Z. G. Chen, Chem. Rev. **120**, 7399–7515 (2020).
[14]S. Xu, M. Hong, X.-L. Shi, M. Li, Q. Sun, Q. Chen, M. Dargusch, J. Zou, and Z.-G. Chen, Energy Environ. Sci. **13**, 3480–3488 (2020).
[15]M. Bharti, A. Singh, S. Samanta, and D. K. Aswal, Prog. Mater. Sci. **93**, 270–310 (2017).
[16]M. Li, M. Hong, M. Dargusch, J. Zou, and Z.-G. Chen, Trends Chem. **3**, 561–574 (2020).
[17]S. Xu, M. Hong, X.-L. Shi, Y. Wang, L. Ge, Y. Bai, L. Wang, M. Dargusch, J. Zou, and Z.-G. Chen, Chem. Mater. **31**, 5238–5244 (2019).
[18]N. Kim, S. Kee, S. H. Lee, B. H. Lee, Y. H. Kahng, Y. R. Jo, B. J. Kim, and K. Lee, Adv. Mater. **26**, 2268–2272 (2014).
[19]O. Bubnova, Z. U. Khan, A. Malti, S. Braun, M. Fahlman, M. Berggren, and X. Crispin, Nat. Mater. **10**, 429–433 (2011).
[20]C. Cho, K. L. Wallace, P. Tzeng, J.-H. Hsu, C. Yu, and J. C. Grunlan, Adv. Energy Mater. **6**, 1502168 (2016).
[21]Q. Yao, Q. Wang, L. Wang, and L. Chen, Energy Environ. Sci. **7**, 3801–3807 (2014).
[22]G. H. Kim, L. Shao, K. Zhang, and K. P. Pipe, Nat. Mater. **12**, 719–723 (2013).
[23]Z. A. Akbar, J.-W. Jeon, and S.-Y. Jang, Energy Environ. Sci. **13**, 2915–2923 (2020).
[24]L. Wang, Z. Zhang, Y. Liu, B. Wang, L. Fang, J. Qiu, K. Zhang, and S. Wang, Nat. Commun. **9**, 3817 (2018).
[25]Q. Jin, S. Jiang, Y. Zhao, D. Wang, J. Qiu, D. M. Tang, J. Tan, D. M. Sun, P. X. Hou, X. Q. Chen, K. Tai, N. Gao, C. Liu, H. M. Cheng, and X. Jiang, Nat. Mater. **18**, 62–68 (2019).
[26]Q. Qin, F. He, and W. Zhang, J. Nanomater. **2016**, 1076158.
[27]Y. Ding, Y. Qiu, K. Cai, Q. Yao, S. Chen, L. Chen, and J. He, Nat. Commun. **10**, 841 (2019).
[28]Y. Lu, Y. Qiu, K. Cai, Y. Ding, M. Wang, C. Jiang, Q. Yao, C. Huang, L. Chen, and J. He, Energy Environ. Sci. **13**, 1240–1249 (2020).
[29]W. Zhou, Q. Fan, Q. Zhang, L. Cai, K. Li, X. Gu, F. Yang, N. Zhang, Y. Wang, H. Liu, W. Zhou, and S. Xie, Nat. Commun. **8**, 14886 (2017).
[30]Q. Zhang, J. Liao, Y. Tang, M. Gu, C. Ming, P. Qiu, S. Bai, X. Shi, C. Uher, and L. Chen, Energy Environ. Sci. **10**, 956–963 (2017).
[31]D. M. Rowe, *Thermoelectrics Handbook: Macro to Nano* (CRC Press, Boca Raton, 2006).
[32]S. Hong, Y. Gu, J. K. Seo, J. Wang, P. Liu, Y. S. Meng, S. Xu, and R. Chen, Sci. Adv. **5**, eaaw0536 (2019).

[33]K. Nan, S. D. Kang, K. Li, K. J. Yu, F. Zhu, J. Wang, A. C. Dunn, C. Zhou, Z. Xie, M. T. Agne, H. Wang, H. Luan, Y. Zhang, Y. Huang, G. J. Snyder, and J. A. Rogers, Sci. Adv. **4**, eaau5849 (2018).
[34]J. Y. Oh, J. H. Lee, S. W. Han, S. S. Chae, E. J. Bae, Y. H. Kang, W. J. Choi, S. Y. Cho, J.-O. Lee, H. K. Baik, and T. I. Lee, Energy Environ. Sci. **9**, 1696–1705 (2016).
[35]L. Francioso, C. De Pascali, I. Farella, C. Martucci, P. Cretì, P. Siciliano, and A. Perrone, J. Power Sources **196**, 3239–3243 (2011).
[36]M. Kim, M. Kim, S. Lee, C. Kim, and Y. Kim, Smart Mater. Struct. **23**, 105002 (2014).
[37]Z. Lu, H. Zhang, C. Mao, and C. M. Li, Appl. Energy **164**, 57–63 (2016).
[38]C. S. Kim, G. S. Lee, H. Choi, Y. J. Kim, H. M. Yang, S. H. Lim, S.-G. Lee, and B. J. Cho, Appl. Energy **214**, 131–138 (2018).
[39]Y. Zhou, S. Zhang, X. Xu, W. Liu, S. Zhang, G. Li, and J. He, Nano Energy **69**, 104397 (2020).
[40]Y. Zhou, Z. Guo, and J. He, Appl. Phys. Lett. **116**, 043904 (2020).